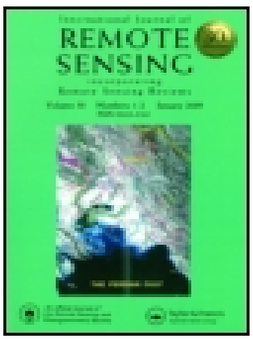

International Journal of Remote Sensing

ISSN: 0143-1161 (Print) 1366-5901 (Online) Journal homepage: http://www.tandfonline.com/loi/tres20

Soil salinity mapping using dual-polarized SAR Sentinel-1 imagery

Mohammad Mahdi Taghadosi, Mahdi Hasanlou & Kamran Eftekhari

To cite this article: Mohammad Mahdi Taghadosi, Mahdi Hasanlou & Kamran Eftekhari (2018): Soil salinity mapping using dual-polarized SAR Sentinel-1 imagery, International Journal of Remote Sensing, DOI: 10.1080/01431161.2018.1512767

To link to this article: https://doi.org/10.1080/01431161.2018.1512767

Published online: 06 Sep 2018.

INTERNATIONAL JOURNAL OF REMOTE SENSING
https://doi.org/10.1080/01431161.2018.1512767

Taylor & Francis
Taylor & Francis Group

Soil salinity mapping using dual-polarized SAR Sentinel-1 imagery

Mohammad Mahdi Taghadosi [a], Mahdi Hasanlou [a] and Kamran Eftekhari [b]

[a]School of Surveying and Geospatial Engineering, College of Engineering, University of Tehran, Tehran, Iran; [b]Department of Soil Genesis, Classification and Cartography, Soil and Water Research Institute, Karaj, Iran

ABSTRACT

Soil salinity is a major environmental threat, which has a negative impact on soil productivity and agricultural fields. One of the most promising methods for monitoring affected areas, which has special importance in land management studies, is through remote sensing technologies. While the potential of optical imagery in detecting saline soils is widely investigated, limited studies have been dedicated to assessing the potential of Synthetic Aperture Radar (SAR) imagery in monitoring soil salinity. Accordingly, this paper deals with soil salinity estimation using Sentinel-1 SAR imagery in an area which is highly affected by salinity hazard. Due to lack of a suitable theoretical model for simulating radar backscatter of soil based on salt contents, we investigated a new method to relate radar intensity to measured in-situ salinity directly. In the first step, Sentinel-1 dual polarized VV (Vertical transmit Vertical receive) and VH (Vertical transmit Horizontal receive) data were acquired from the study site. A field study was also conducted, simultaneously, and the Electrical Conductivity (EC) of several soil samples was measured. We then extracted some features based on the intensity images of both VV and VH polarization. Based on the fact that the target texture affects the radar response, an analysis of the texture was also performed by calculating the first and second order statistics, extracted from the histogram and Gray Level Co-occurrence Matrix (GLCM), respectively. The Support Vector Regression (SVR) technique, with different kernel functions, was used to relate explanatory variables to ground measured salinity. We also applied Feature Selection (FS) algorithms of the Genetic Algorithm (GA) and Sequential Feature Selection (SFS) for optimizing the model and selecting the best explanatory features. The results showed that ε-SVR with Radial Basis Function (RBF) kernel had the most accuracy with the Coefficient of Determination (R^2) = 0.9783 and Root Mean Square Error (RMSE) = 0.3561 when the GA FS was applied. Also $G_{FO,VV}$ and R_{VH} had the best performance in salinity detection. It can be concluded that the intensity images of VV and VH polarization of SAR imagery have the potential to discriminate saline surface soils, regardless of the failure of common backscattering models.

ARTICLE HISTORY
Received 1 February 2018
Accepted 2 August 2018

CONTACT Mahdi Hasanlou hasanlou@ut.ac.ir School of Surveying and Geospatial Engineering, College of Engineering, University of Tehran, P. O. Box:11155-4563, Postal Code:1439957131 Tehran, Iran

1. Introduction

Salinization is one of the most hazardous environmental phenomena which leads to desertification and loss of agricultural productivity (Metternicht and Zinck. 2009; Shrestha and Farshad 2009; Allbed and Kumar 2013). The extent and severity of this problem have become more serious over the last years, which makes it inevitable to find an effective approach for managing affected lands. Remote sensing technology is one of the most promising and cost-effective tools, which can be used to monitor soil salinity problems (Singh et al. 2010; Elhag 2016; Allbed and Kumar 2013; Brunner et al. 2007). Most of the research in this field has been dedicated to assessing the potential of optical remote sensing for managing affected areas, which can be correctly recognized through high spectral reflectance of the visible and near-infrared range of the electromagnetic spectrum. However, for soils with dark colored surface layers and also over coastal areas where the soil surface is highly affected by moisture content, optical imagery provides inaccurate results (Aly, Bonn, and Magagi 2007; Saha 2011; Li et al. 2013).

Due to the limitation of optical satellite sensors in detecting salinity and also the sensitivity of the signal to dielectric properties of materials in microwave wavelengths, Synthetic Aperture Radar (SAR) imagery can be more reliable for salinity monitoring. Theoretically, microwave remote sensing has great potential for assessing soil salinity and mapping the affected regions (Aly, Bonn, and Magagi 2007; Li et al. 2013; Gong et al. 2013). However, few studies have investigated the potential of SAR imagery for salinity monitoring (Saha 2011; Barbouchi et al. 2015). Radar backscattering is mostly influenced by two main factors: (1) sensor parameters, namely wavelength (λ), polarization (p), incidence angle (Θ), and (2) target parameters such as surface roughness, slope orientation, and dielectric properties of a target (Wu and Wang 2011; MirMazloumi and Sahebi 2016). Among these parameters, complex dielectric constant of a substance, which is an intrinsic property of a material (Hasar, Akay, and Kharkovsky 2003), plays an important role in determining radar backscatter, so that, simulating and evaluating this parameter, in both real and imaginary part, has been taken into consideration in a number of studies (Li et al. 2014; Lasne et al. 2008; Bell et al. 2001; Wu and Wang 2011).

The key parameters in determining the dielectric properties of a material are (1) moisture content, which specifies permittivity (or real part;ε'), and (2) the ionic conductivity, which markedly affects loss factor (or imaginary part;ε'') (Behari 2005). Accordingly, it can be interpreted that existence of salt in the soil solution has a direct effect on the dielectric constant (especially in loss factor), and radar backscattering values. Generally, defining a relationship between three components of the conductivity of a material (moisture and salinity), dielectric constant, and radar backscattering (sigma-naught;σ^0) has a crucial role in detecting salinity using radar remote sensing, the subject, which has been addressed in the previous research. Wu and Wang (2011) simulated the effect of moisture and salinity on dielectric constant and the backscattering coefficient of VV (Vertical transmit Vertical receive) and HH (Horizontal transmit Horizontal receive) polarization using a theoretical Advanced Integral Equation Model (AIEM). The results of this study showed that the imaginary part of the dielectric constant increases with salinity. They also concluded that the backscattering coefficient of VV and HH polarization is influenced by both soil salinity

and moisture, which can be used to retrieve soil salinity, especially when the soil moisture is low. In a case study in western Jilin Province, Li et al. (2014) used the backscattering model AIEM to evaluate the behaviours of the backscattering coefficient in salt-affected soils. Combined Dobson mixing model and seawater dielectric constant model were also used to estimate the effect of salinity and moisture on the dielectric constant. The results of this study revealed the potential of using RADAR SATellite-2 (RADARSAT-2) data to measure soil salinity; however, they confirmed that there is no suitable model to estimate the backscattering coefficient based on changes in salinity values. Lasne et al. (2008) assessed the effect of salinity on the permittivity of geological materials, using dielectric mixing models. They also simulated the radar backscattering coefficient across different range frequencies (1–7 GHz) using analytical scattering models Integral Equation Model (IEM) and Small Perturbation Model (SPM). They concluded that the sensitivity of the backscattering coefficient to the salt values relies on the moisture content, which is more obvious in VV polarization. Aly, Bonn, and Magagi (2007) used several backscattering models to assess the effect of salinity on the backscattering coefficient. Four RADARSAT-1 data in standard modes were acquired to be used for validation of proposed backscatter models. The results of this study showed that high values of the dielectric constant, due to the salt presence, has a significant effect on the radar backscattering coefficient. Shao et al. (2003) assessed the real and imaginary parts of the dielectric constant of soils, which were artificially moistened and salinized, as a function of salinity, moisture and microwave frequency. The results showed that the real part of the dielectric constant is strongly influenced by soil moisture, while the imaginary part is strongly affected by both moisture and salinity, especially at low frequencies. They also concluded that the C and L bands of the radar data are more suitable for detecting salinity, due to the greater sensitivity of the imaginary part of the dielectric constant to soil salinity in these frequencies.

However, a review of the results of previous research shows that developing a theoretical model, which properly relates the salinity to complex dielectric constant and backscattering in different polarization modes, has not yet become possible. Since most of the backscattering models like Dubois Model (DM), SPM, Physical Optical Model (POM), and IEM only consider the effects of moisture in the soil for modelling, an evaluation of the effects of salinity on these models cannot be observed. In this regard, a few studies attempted to change these models by adding conductivity of salty water instead of free water in order to assess the effect of salinity on modelling the dielectric behaviour of the material and its effect on the backscattering coefficient. However, the results of these studies were not satisfactory, which indicate that the available theoretical model is not adequate for monitoring salinity by radar remote sensing.

Despite the problems in modelling salinity and relating soil salinity values to radar satellite data, a direct relationship between Electrical Conductivity (EC) of soils, and backscattering image has been proven in some cases. Aly, Bonn, and Magagi (2007) proposed a parametric formulation to determine salinity from RADARSAT-1 data, without a backscattering model. The linear regression analysis was performed, and a good relationship was observed between the measured salinity of the soil samples and the radar images, with a coefficient of determination (R^2) of 0.8300. Moreover, in a case study in the Kairouan region of central Tunisia, Grissa et al. (2011) developed an

empirical model to map soil salinity using intensity images of ENVIronmental SATellite (ENVISAT) data in VV and HH polarization. The Support Vector Machine (SVM) based classifier was used to generate a salinity map with three classes of salinity. The results of this study were satisfactory, however, more soil samples should have been used for model validation.

Furthermore, due to the impact of the soil texture on the radar response, which is described by Dobson and Ulaby (1981) and also the distinct texture of saline surface soils in affected areas, extraction of texture features from satellite data may be useful for soil salinity estimation by radar imagery. The possibility of using texture analysis for salinity detection will be also discussed in this paper.

Given the issues raised above, this paper aims to assess the possibility of using radar imagery to detect salinization. Since the theoretical and empirical models have not been able to accurately identify the effects of salinity on signal and simulate the dielectric behaviour of salt composites, this study attempts to investigate a new method for a direct relationship between soil salinity values, measured in-situ, and the backscatter of the radar signal from SAR imagery. For this purpose, the Sentinel-1 dual polarized SAR imagery, which is freely available, is acquired. Owing to the fact that the Sentinel-1 satellite provides continuous imagery of the earth's surface (day and night and in all weather conditions) with a high spatial and temporal resolution (Torres et al. 2012; Fletcher 2012), investigating a direct way to retrieve soil salinity allows us to monitor affected regions in different climate areas at all times of the year and various time intervals. Furthermore, using the direct way to characterise salinity does not need to obtain soil parameters such as volumetric soil moisture (m_v), soil surface temperature (T_s), bulk or specific density (ρ_b, ρ_s), percentage of soil particles, etc., which are used for simulating complex dielectric constant, and also it does not require to assess validity domain of backscattering models (DM, SPM, POM, etc.). This methodology will now be discussed in more detail.

2. Materials and methods

2.1. *Study area and datasets*

Kuh Sefid is a village located in the Central District of Qom County, Qom, Iran. This area, which has a hot and dry climate with annual precipitation of about 115.5 mm, the highest temperature of 39.7°C in July and the lowest temperature of 0.4°C in December, is affected by severe salinity hazard mainly due to the vicinity to the Salt Lake Qom. The surface soil texture in this region varies between silt loam to silty clay loam, which has a yellowish brown to dark brown colour (Fallahi, Banaei, and Eskandarzadeh 1983). From this region, several soil samples were taken and their salinity was measured to be used as ground truth data.

The Sentinel-1 SAR imagery, in the Interferometric Wide (IW) mode, C-band, with dual polarization VV (Vertical transmit Vertical receive), VH (Vertical transmit Horizontal receive), was acquired on 1 March 2017, in coincidence with field observations. Figure 1 shows the Kuh Sefid district image and distribution of the soil samples in the study site, obtained from Google Earth imagery. The colour composite image of the Sentinel-1 data in this region (Red: VV, Green: VH, Blue: VH/VV) is also shown in Figure 2.

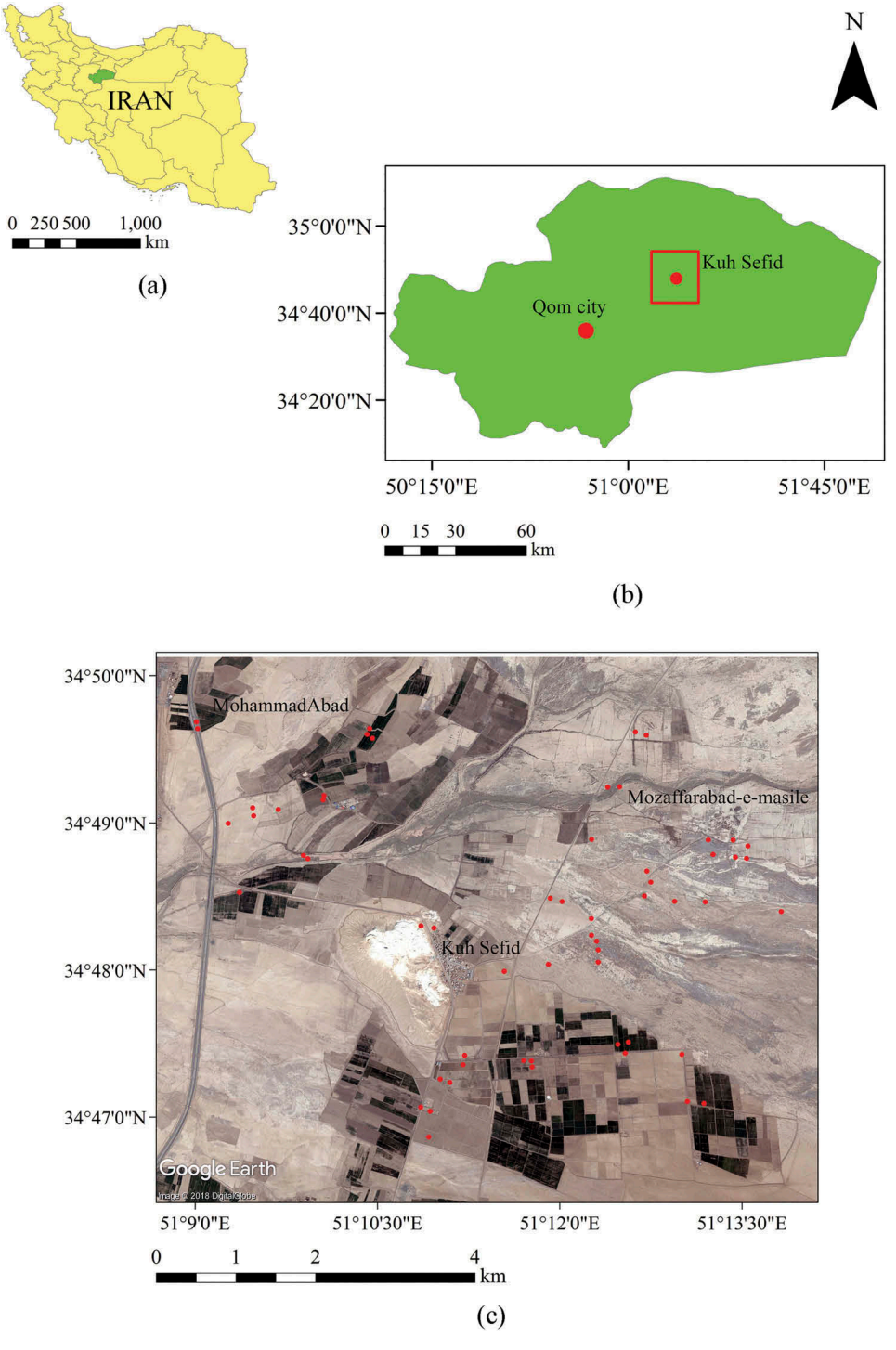

Figure 1. (a) Location of Qom County in Iran, (b) Location of Kuh Sefid in the central district of Qom County, (c) Kuh Sefid district image acquired from Google Earth and distribution of the soil samples in the study site.

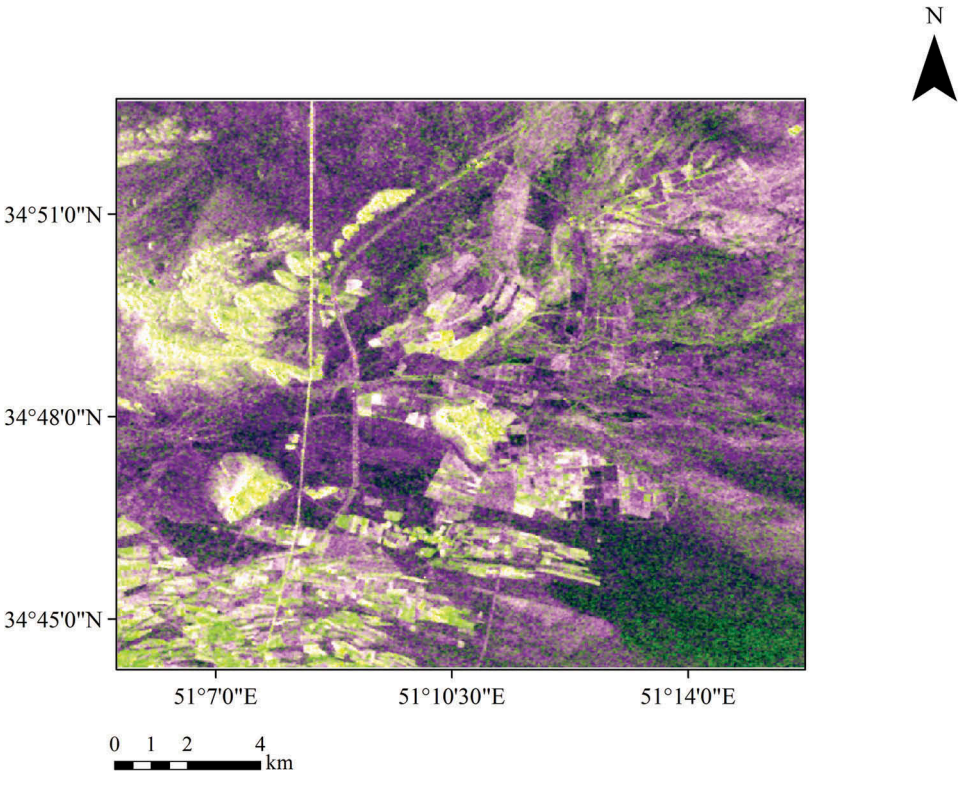

Figure 2. The colour composite image of the Sentinel-1 data from Kuh Sefid region (Red: VV, Green: VH, Blue: VH/VV).

2.2. *Field investigation and measuring salinity*

The field observations were carried out on 4 March 2017, and 58 soil samples were randomly collected. Soil samples were then analysed in the laboratory, and the EC of samples was measured. For this purpose, the method of measuring the electrical conductivity of the soil-water extract, with a fixed soil solution ratio of 1:1, proposed by Richards (1954), was used and the conductivity of solution was measured by Conductivity Pocket metre (WTW Cond 330i) at 25.0°C. The spatial location of soil samples and their corresponding measured EC, in unit of decisiemens per meter (dS m^{-1}), were stored to be used as ground-truth data. These image and ground-truth data sets can be found online in (Remote Sensing Laboratory 2018).

2.3. *Used methodology*

Since the single-phase image of SAR imagery, which can be derived from the Single Look Complex (SLC) data of Sentinel-1, does not provide any information to be used for salinity detection, only the intensity of the Sentinel-1 product was considered for analysis. The phase information can be applied to studies in which the temporal changes of salinity would be estimated by the interferometry SAR (InSAR) technique as discussed in Barbouchi et al. (2015).

Accordingly, data preparation was firstly performed through several pre-processing steps: radiometric calibration, speckle filtering, and geometric and terrain correction. Then, sigma-naught images in both VV and VH polarization were derived according to Lee and Pottier (2009). In addition to single images of sigma-naught, amplitude images in both polarization and also the ratio between VV and VH backscattering images were extracted, as shown in Table 1, to assess whether it contained valuable information for salinity detection.

In addition to mentioned features, which were extracted from radar intensity, texture analysis based on radar images in two polarization modes was performed to assess its potential to detect saline surface soils. Image-based texture features which specify the spatial distribution of radar brightness values in the image can be used to discriminate affected regions. Therefore, texture features were extracted by calculating histogram-based features, from first-order statistics and also second-order statistics extracted from the Gray Level Co-occurrence Matrix (GLCM) that considers the relative position of the pixels with respect to each other (Vijayarekha 2014). Table 1 shows all the features that were extracted for analysis with their formula.

where A and I refer to Amplitude and Intensity of SAR image, $E_{0,x}$ and $E_{0,y}$ are the electric field in the x and y direction, σ^0 is the averaged radar cross section per unit area,

Table 1. Extracted features from radar intensity and analysis of textures.

	Name	Formula	Source
Radar Intensity	Amplitude	$A = \sqrt{E^2{}_{0,x} + E^2{}_{0,y}}$	(Lee and Pottier 2009)
	Sigma-naught	$\sigma^0 = \frac{4\pi r^2}{A_0}\frac{\lvert E_S{}^2\rvert}{\lvert E_I\rvert^2}$	(Lee and Pottier 2009)
	Ratio	$\sigma^0{}_{VH}/\sigma^0{}_{VV}$, I_{VH}/A_{VV}, I_{VV}/A_{VH}	(Chunming et al. 2005; Lee et al. 1994)
Histogram-Based Textures (first order)	Mean	$= \sum_{i=1}^{N_g} ip(i)$	(Materka and Strzelecki 1998; Vijayarekha 2014)
	Variance	$\sigma^2 = \sum_{i=1}^{N_g} (i-)^2 p(i)$	(Materka and Strzelecki 1998; Vijayarekha 2014)
	Skewness	$s = \sigma^{-3} \sum_{i=1}^{N_g} (i-)^3 p(i)$	(Materka and Strzelecki 1998; Vijayarekha 2014)
	Kurtosis	$k = \sigma^{-4} \sum_{i=1}^{N_g} (i-)^4 p(i) - 3$	(Materka and Strzelecki 1998; Vijayarekha 2014)
	Entropy	$E_{FO} = -\sum_{i=1}^{N_g} p(i)\log_2 p(i)$	(Materka and Strzelecki 1998; Vijayarekha 2014)
	Energy	$G_{FO} = \sum_{i=1}^{N_g} p(i)^2$	(Materka and Strzelecki 1998; Vijayarekha 2014)
Grey Level Co-occurrence Matrix Textures (second order)	Correlation	$R = \sum_{i=1}^{N_g}\sum_{j=1}^{N_g} \frac{(i-_x)(j-_y)p(i,j)}{\sigma_x\sigma_y}$	(Materka 1998; Vijayarekha 2014)
	Contrast	$C = \sum_{i=1}^{N_g}\sum_{j=1}^{N_g} \lvert i-j\rvert^2 p(i,j)$	(Materka and Strzelecki 1998; Vijayarekha 2014)
	Homogeneity	$H = \sum_{i=1}^{N_g}\sum_{j=1}^{N_g} \frac{p(i,j)}{1+\lvert i-j\rvert^2}$	(Materka and Strzelecki 1998; Vijayarekha 2014)
	Dissimilarity	$D = \sum_{i=1}^{N_g}\sum_{j=1}^{N_g} \lvert i-j\rvert p(i,j)$	(Materka and Strzelecki 1998; Vijayarekha 2014)
	Entropy	$E_{SO} = \sum_{i=1}^{N_g}\sum_{j=1}^{N_g} [p(i,j)]^2$	(Materka and Strzelecki 1998; Vijayarekha 2014)
	Energy	$G_{SO} = -\sum_{i=1}^{N_g}\sum_{j=1}^{N_g} p(i,j)\log_2[p(i,j)]$	(Materka and Strzelecki 1998; Vijayarekha 2014)

E_I and E_S are the incident electromagnetic wave and the scattered wave, respectively. $p(i)$ is a first order probability, which defines as $p(i) = N_i/M$, N_i is the number of pixels of grey value i in the window, M is the total number of pixels in the neighbourhood window of specified size centred around the pixel. N_g is the total number of grey levels in the image, $p(i,j)$ is a second-order joint probability of two pixels i and j, $\sigma_x$andσ_y are the standard deviations of the row and column sums of the GLCM.

Based on the spatial location of the soil samples, the corresponding pixel values from all the described features were extracted to be used for relating ground measured salinity and Sentinel-1 derived features. The Support Vector Regression (SVR) algorithm, proposed by Vapnik, Golowich, and Smola (1996), was used to evaluate the possibility of creating a direct relationship between measured soil EC and corresponding satellite features. Since the SVR maps the input data on to a higher dimensional feature space, it can be more applicable than other regression techniques, especially in non-linear cases. Different Kernel functions which include (1) Linear, (2) Polynomial in different degrees, and (3) (Gaussian) Radial Base Function (RBF), from the ε-SVR model, were selected to be used in the analysis. In order to achieve a better model fit, the optimization processes should be performed for each model, which is considered in two main steps: First, the Parameter Selection of ε-SVR, that was done for selecting a parameter of each kernel function and was based on all explanatory variables. Second, the Feature Selection techniques for improving the model performance and selecting the best features. It is important that the selected parameters from the first step remain unchanged for comparing the constructed models. The Genetic Algorithm (GA) and Sequential Feature Selection (SFS) methods were applied for feature selection by criteria of minimizing Root Mean Square Error (RMSE) and maximizing coefficient of determination (R^2) values. Based on the results of the analysis, the constructed models were used to map soil salinity for all the scene. Figure 3 indicates the flowchart of the proposed method.

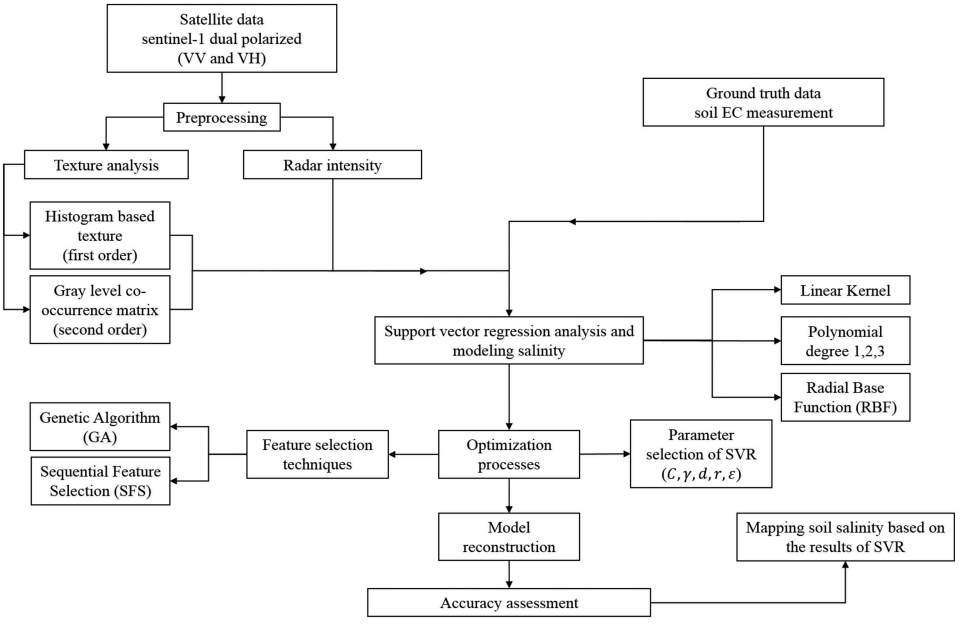

Figure 3. Flowchart of the proposed method.

As can be seen in the flowchart of Figure 3, various features were extracted from the texture analysis and the intensity of the radar in the VV and VH polarization of Sentinel-1 data in the study site. Salinity was also measured for several soil samples in the Kuh Sefid region. The SVR technique with different kernel functions was used to relate measured salinity to corresponding explanatory variables, including radar intensity features and image-based texture features. The optimization processes were also performed by Parameter Selection of ε-SVR and Feature Selection algorithms (GA and SFS). Based on the obtained results and performing the accuracy assessment, the constructed models are used for estimating the salinity map of the study site.

3. Results and discussion

3.1. *Model building and validation*

3.1.1. *Remove bad features*

Evaluating the 31 feature images that were extracted from the VV and VH polarization of Sentinel-1 data, indicated that some features are not suitable for analysis. Some of them had similar values in the image, which makes it difficult to retrieve salinity from them. Some others were noisy in both polarization modes and there was no apparent relationship between the extracted features and the measured salinity values. Based on the observations, inappropriate features were excluded from the data cube and the SVR technique was performed, with 19 features, to relate Sentinel-1 (VV and VH) data and its derived features to measured soil EC values.

3.1.2. *Data splitting and optimization procedures*

To run the algorithm, the data cube was divided into two separate parts: the train (70%) and the test (30%) data, which were used for model building and validation, respectively. In the first step, the parameter optimization of ε-SVR was done for each kernel function. Table 2 shows the selective parameter of each kernel and their estimated values. In the second phase, GA and SFS were performed on the data and the best features were selected. Table 3 shows the GA parameters which were used for selecting and processing the features. The search process of GA for different kernel function of SVR is also shown in Figure 4.

3.1.3. *Accuracy assessment*

The analysis was performed to estimate the soil EC from the radar backscattering of Sentinel-1 data, and accuracy assessment was done based on R^2, RMSE, and Normalized Root Mean Square Error (NRMSE) values obtained from the ε-SVR method. The results of

Table 2. Kernel functions and their selective parameters of SVR.

Kernel Function	Formula	Selective parameter
Linear	$x^{\mathrm{T}}y$	$C = 1.000, \varepsilon = 0.100$
Polynomial (degree 1)	$(\gamma x^{\mathrm{T}}y + r)^{\mathrm{d}}$	$d = 1,\ C = 11.313, \gamma = 0.088,\ r = 5.656,\ \varepsilon = 0.100$
Polynomial (degree 2)		$d = 2,\ C = 0.500, \gamma = 0.044,\ r = 0.353,\ \varepsilon = 0.100$
Polynomial (degree 3)		$d = 3,\ C = 0.031, \gamma = 0.031,\ r = 0.031,\ \varepsilon = 0.100$
Radial Base Function (Gaussian)	$\exp(-\gamma x - y^2)$	$C = 8.000, \gamma = 0.004, \varepsilon = 0.062$

Table 3. Incorporated GA parameters.

Parameter	Value
Population size: specifies how many individuals there are in each generation.	20
Elitism ratio: specifies the number of individuals that are guaranteed to survive to the next generation.	1
Crossover fraction: specifies the fraction of the next generation.	0.7
Crossover method	one point
Mutation ratio: specifies how the genetic algorithm makes small random changes in the individuals in the population to create mutation children.	0.05
Maximum generation: specifies the maximum number of iterations for the genetic algorithm to perform.	100

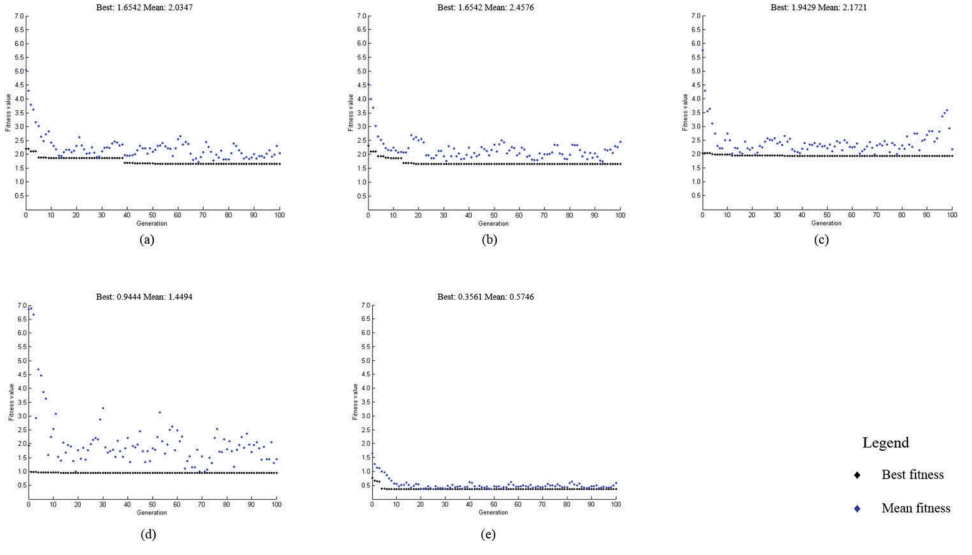

Figure 4. Search process of GA for different kernel function of SVR, (a) Linear, (b) Poly degree 1, (c) Poly degree 2, (d) Poly degree 3, and (e) RBF.

the regression analysis and accuracy assessments for different kernel functions is shown in Table 4. In addition, the optimal features that were selected based on FS processing were also presented.

3.1.4. *Generating soil salinity maps*

The results of regression models were used to generate salinity maps of the study site. For each kernel function, three salinity maps were generated based on (1) all explanatory variables, (2) selected variables of SFS, and (3) selected variables of GA. Figures 5–7 show estimated salinity maps for each kernel function of ε-SVR.

The obtained results are as follows:

(1) The obtained results from ε-SVR with different kernel functions indicate that the best accuracy is provided by Gaussian (RBF) kernel with R^2 = 0.9783 and RMSE = 0.3561 when the GA Feature Selection is applied. This reveals the more efficiency of RBF kernel function than other ε-SVR kernels. Moreover, the comparison between optimization algorithms shows that GA is more efficient

Table 4. Accuracy assessment of constructed models.

SVR Kernel function	Feature selection algorithm	Train/ Test	*R*2	RMSE	NRMSE	Selected feature
Linear Kernel	– –	Test	0.8674	2.9535	0.3903	All
		Train	0.8569	1.2459	0.1572	
	SBS	Test	0.6720	1.8666	0.2467	H_{VV}, $G_{FO,VV}$, R_{VV}, H_{VH}, $G_{FO,VH}$, R_{VH}, σ^0_{VH}, σ^0_{VV}, A_{VH}, A_{VV}, I_{VH}/A_{VV}
		Train	0.3729	2.8850	0.3640	
	GA	Test	0.7303	1.6543	0.2186	$G_{FO,VV}$, H_{VH}, $G_{FO,VH}$, $E_{FO,VH}$, R_{VH}, I_{VH}/A_{VV}
		Train	0.5829	2.2583	0.2849	
Polynomial Kernel degree 1	– –	Test	0.8674	2.9533	0.3903	All
		Train	0.8569	1.2459	0.1572	
	SBS	Test	0.6720	1.8666	0.2467	H_{VV}, $G_{FO,VV}$, R_{VV}, H_{VH}, $G_{FO,VH}$, R_{VH}, σ^0_{VH}, σ^0_{VV}, A_{VH}, A_{VV}, I_{VH}/A_{VV}
		Train	0.3729	2.8850	0.3640	
	GA	Test	0.7303	1.6542	0.2186	$G_{FO,VV}$, H_{VH}, $G_{FO,VH}$, $E_{FO,VH}$, R_{VH}, I_{VH}/A_{VV}
		Train	0.5829	2.2583	0.2849	
Polynomial Kernel degree 2	– –	Test	0.9194	2.4923	0.3293	All
		Train	0.8173	1.4424	0.1820	
	SBS	Test	0.9185	2.1823	0.2884	D_{VV}, $E_{FO,VV}$, $_{VV}$, R_{VV}, $E_{FO,VH}$, $_{VH}$, R_{VH}, σ^0_{VH}, σ^0_{VV}, A_{VH}, A_{VV}, $\sigma^0_{VH}/\sigma^0_{VV}$, I_{VH}/A_{VV}
		Train	0.8142	1.4543	0.1835	
	GA	Test	0.9002	1.9428	0.2567	$G_{FO,VV}$, $E_{FO,VV}$, $_{VV}$, $G_{FO,VH}$, $_{VH}$, A_{VH}, I_{VH}/A_{VV}
		Train	0.7615	1.6276	0.2053	
Polynomial Kernel degree 3	– –	Test	0.6223	2.4314	0.3213	All
		Train	0.7647	1.6241	0.2049	
	SBS	Test	0.9545	0.9444	0.1248	$G_{FO,VV}$, $E_{FO,VV}$, $_{VV}$, R_{VV}, $G_{FO,VH}$, $E_{FO,VH}$, R_{VH}, σ^0_{VH}, σ^0_{VV}, A_{VH}, A_{VV}, $\sigma^0_{VH}/\sigma^0_{VV}$, I_{VH}/A_{VV}, I_{VH}/A_{VV}
		Train	0.5535	2.1603	0.2725	
	GA	Test	0.9545	0.9444	0.1248	$G_{FO,VV}$, $E_{FO,VV}$, $_{VV}$, R_{VV}, $G_{FO,VH}$, $E_{FO,VH}$, R_{VH}, σ^0_{VH}, σ^0_{VV}, A_{VH}, A_{VV}, $\sigma^0_{VH}/\sigma^0_{VV}$, I_{VH}/A_{VV}, I_{VH}/A_{VV}
		Train	0.5535	2.1603	0.2725	
RBF Kernel	– –	Test	0.9297	0.6651	0.0879	All
		Train	0.7396	1.9166	0.2418	
	SBS	Test	0.9783	0.3561	0.0471	$G_{FO,VV}$, $E_{FO,VV}$, $_{VV}$, $E_{FO,VH}$, $_{VH}$, σ^0_{VV}, A_{VV}
		Train	0.7324	1.9941	0.2516	
	GA	Test	0.9783	0.3561	0.0471	$G_{FO,VV}$, $E_{FO,VV}$, $_{VV}$, $E_{FO,VH}$, $_{VH}$, σ^0_{VV}, A_{VV}
		Train	0.7324	1.9941	0.2516	

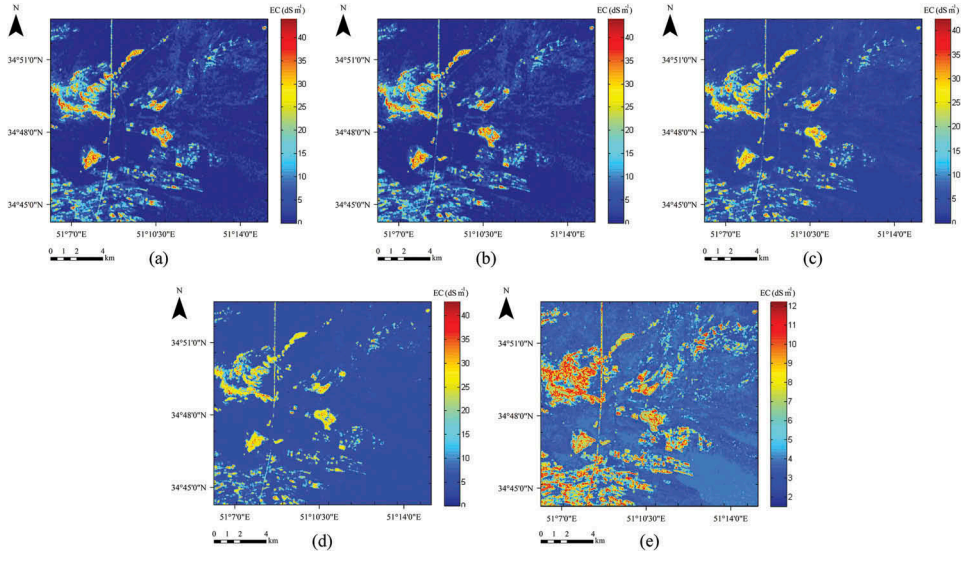

Figure 5. Result of EC mapping using SVR model with all input features in different kernels, (a) linear kernel, (b) polynomial kernel degree 1, (c) polynomial kernel degree 2, (d) polynomial kernel degree 3, and (e) radial base function.

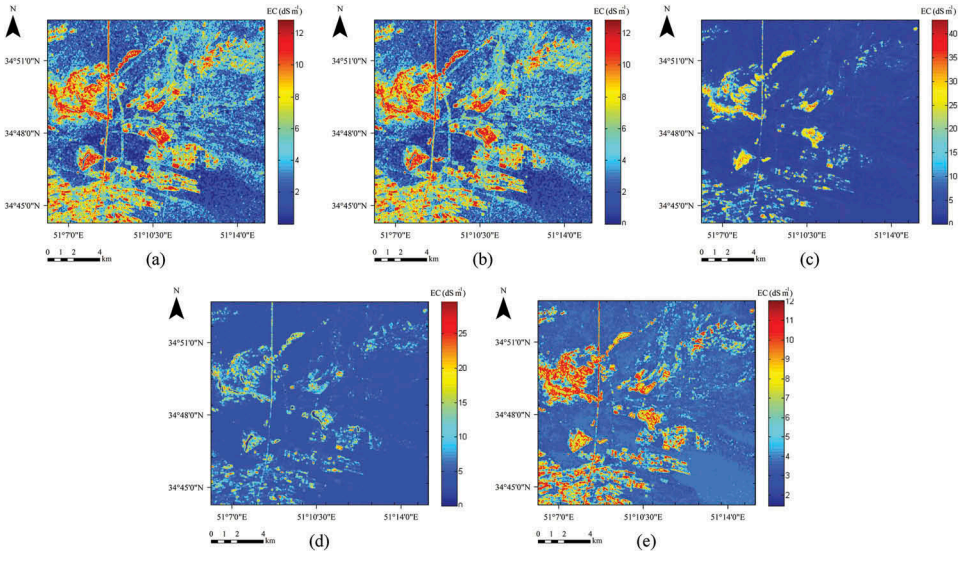

Figure 6. Result of EC mapping using SVR model with GA feature selection in different kernels, (a) linear kernel, (b) polynomial kernel degree 1, (c) polynomial kernel degree 2, (d) polynomial kernel degree 3, and (e) radial base function.

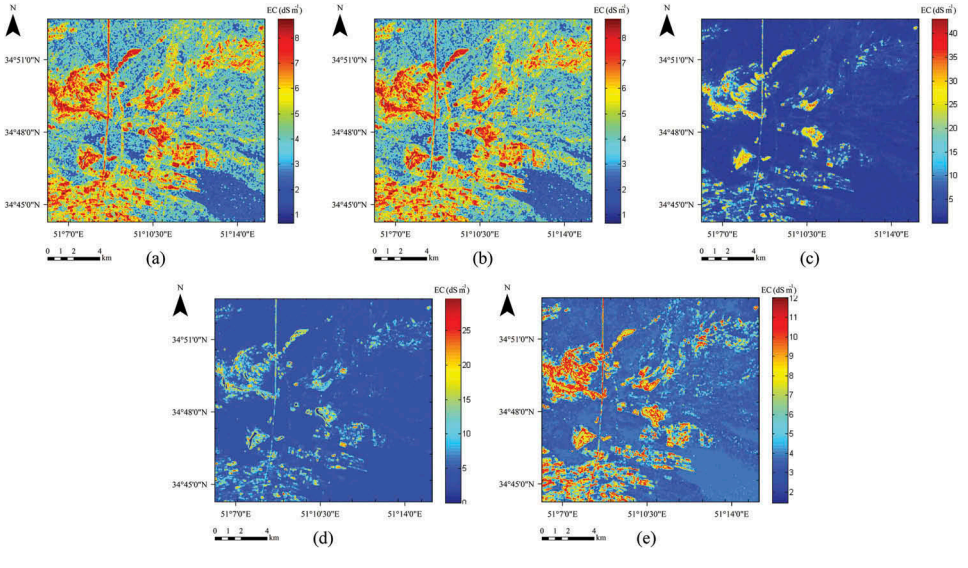

Figure 7. Result of EC mapping using SVR model with SFS feature selection in different kernels, (a) linear kernel, (b) polynomial kernel degree 1, (c) polynomial kernel degree 2, (d) polynomial kernel degree 3, and (e) radial base function.

than SFS due to providing fewer number of selected features and lower RMSE values in most of the kernel functions.

(2) The predicted EC maps obtained from different input features and various kernel functions represent a relatively uniform pattern within the study site. This pattern shows high salt contents in the central parts of the Kuh Sefid. The

soil EC values have gradually declined with increasing the distance from the central parts of the Kuh Sefid; however, the decrease in east part of the Kuh Sefid is more sharply and high EC values can be seen in some parts of the west and north-west of the site.

(3) Comparison of generated soil EC maps provided by different kernel functions reveals that using degree 2 polynomial kernel function increases the range of variation of EC values in the scene from 0 dS m^{-1} to 40 dS m^{-1}, producing intensified salinity maps. Increasing the range of EC variations is also observed in other kernel functions when all explanatory variables are used (SVR with Gaussian kernel being an exception) which may be due to large number of input features.

(4) Evaluating the generated salinity maps obtained by linear and degree 1 polynomial kernel functions shows high similarity between EC maps in all three cases. This similarity can also be observed in their calculated R^2-RMSE values and also their optimum selected features, as shown in Table 4. Although the spatial pattern of predicted EC values in these maps are fairly similar to others, a dramatic fluctuation can be observed in EC values all over the scene, which leads to producing noisy maps. The calculated R^2 values in both kernels are also lower than other cases when optimization algorithms (GA and SFS) were used, confirming that their corresponding EC maps are less reliable.

3.2. *Discussion*

The results of the present study, performed to retrieve soil salinity from Sentinel-1 SAR imagery by using ε-SVR technique and analysis of texture, revealed the following main findings:

(1) The backscatter image of Sentinel-1 radar imagery in the VV and VH polarization modes alongside an analysis of texture features (first- and second-order), have great potential to estimate soil salinity in microwave wavelengths, regardless of the failure of common backscattering models and soil moisture content. This indicates that radar intensity and its derived texture images have valuable information, which can be used for monitoring salinity.

(2) Although the theoretical and empirical models are unable to simulate radar backscatter of salt-affected regions and relate salinity values to radar response, developing a direct relationship between intensity values of the VV and VH polarization of Sentinel-1 data and in-situ salinity measurements is provided in this study by using ε-SVR. This represents the ε-SVR as a powerful regression technique for model building, especially when the case is non-linear.

(3) Applying various decomposition techniques to Polarimetric SAR data, which provides new features with different characteristics, may be useful for detecting salinity based on radar signal. However, since the Sentinel-1 data is a dual polarized (VV and VH) radar instrument, evaluating the effect of decomposition product for salinity detection was not applicable to this study. An assessment of the potential of quad-pol SAR data for detecting salinity in future studies is highly recommended. We also did not take account of the phase information, which

could be extracted from Sentinel-1 data, since the single-phase image is a random noise and does not provide any information. Phase information can be more practical in multi-year studies of salinity when salt-affected regions change with time and temporal changes in soil conductivity may appear through the InSAR technique as discussed in Barbouchi et al. (2015).

(4) Although the obtained results show good performance in estimating salinity, and the constructed models are valid in most of the kernel functions, the applied models are not fully generalizable yet. Given the fact that the radar backscattering is influenced by soil conductivity, developing a theoretical model to relate salinity, soil moisture, complex dielectric constant and radar signal, is a pivotal task.

4. Conclusion

This paper has focused on evaluating the potential of dual polarized SAR imagery in monitoring soil salinity. Due to lack of a proper backscattering model for simulating radar backscatter of soil based on salt content, less attention has been paid to use Radar remote sensing for salinity monitoring, and most of the researches in this field have been dedicated to evaluate the spectral behaviour of salt-affected soils in the visible and near-infrared range of the electromagnetic spectrum. However, assessing the possibility of using radar imagery to retrieve soil salinity and creating a relationship between measured soil salinity and radar data have special importance, helping to cover the weakness of the developed backscattering models in this field. Accordingly, this study aimed to investigate the direct relationship between measured salinity (EC) and radar images, provided by the Sentinel-1 SAR satellite. To this purpose, intensity images in VV and VH polarization and also image-based texture features were extracted from satellite data to be used as explanatory variables. Model building was performed using the ε-SVR techniques, and the best result was provided by the Gaussian kernel when GA utilized for the optimization process. The results of this study revealed that although simulating the radar backscatter of soil performed by backscattering models has been failed in salt-affected regions, SAR data has enough capability to discriminate saline soils directly. This study can be considered as a starting point for further exploitation of SAR imagery in soil salinity monitoring. Utilizing the potential of quad-polarized SAR images in different frequency bands (P, L, C, X) and also applying various decomposition techniques to SAR data for generating salinity models is recommended for future studies.

Disclosure statement

No potential conflict of interest was reported by the authors.

ORCID

Mohammad Mahdi Taghadosi http://orcid.org/0000-0003-0773-1570
Mahdi Hasanlou http://orcid.org/0000-0002-7254-4475

References

Allbed, A., and L. Kumar. 2013. "Soil Salinity Mapping and Monitoring in Arid and Semi-Arid Regions Using Remote Sensing Technology: A Review." *Advances in Remote Sensing* 2013 (Dec). doi:10.4236/ars.2013.24040.

Aly, Z., F. J. Bonn, and R. Magagi. 2007. "Analysis of the Backscattering Coefficient of Salt-Affected Soils Using Modeling and RADARSAT-1 SAR Data." *IEEE Transactions on Geoscience and Remote Sensing* 45 (2): 332–341. doi:10.1109/TGRS.2006.887163.

Asfaw, E., K. V. Suryabhagavan, and M. Argaw. 2016. "Soil Salinity Modeling and Mapping Using Remote Sensing and GIS: The Case of Wonji Sugar Cane Irrigation Farm, Ethiopia." *Journal of the Saudi Society of Agricultural Sciences*. Accessed February 24 2017. doi:10.1016/j.jssas.2016.05.003.

Barbouchi, M., R. Abdelfattah, K. Chokmani, N. B. Aissa, R. Lhissou, and A. E. Harti. 2015. "Soil Salinity Characterization Using Polarimetric InSAR Coherence: Case Studies in Tunisia and Morocco." *IEEE Journal of Selected Topics in Applied Earth Observations and Remote Sensing* 8 (8): 3823–3832. doi:10.1109/JSTARS.2014.2333535.

Behari, J. 2005. *Microwave Dielectric Behaviour of Wet Soils*.2005 ed. New York: New Delhi: Springer. doi:10.1007/1-4020-3288-9.

Bell, D., C. Menges, W. Ahmad, and J. J. Van Zyl. 2001. "The Application of Dielectric Retrieval Algorithms for Mapping Soil Salinity in a Tropical Coastal Environment Using Airborne Polarimetric SAR." *Remote Sensing of Environment* 75 (3): 375–384. doi:10.1016/S0034-4257(00)00180-2.

Brunner, P., H. T. Li, W. Kinzelbach, and W. P. Li. 2007. "Generating Soil Electrical Conductivity Maps at Regional Level by Integrating Measurements on the Ground and Remote Sensing Data." *International Journal of Remote Sensing* 28 (15): 3341–3361. doi:10.1080/01431160600928641.

Chunming, H., G. Huadong, S. Yun, and L. Jingjuan. 2005. "Classification of ASAR Images Based on Texture." *Proceedings. 2005 IEEE International Geoscience and Remote Sensing Symposium, 2005. IGARSS '05.*, 3849–3851. 6. doi:10.1109/IGARSS.2005.1525749.

Dobson, M. C., and F. Ulaby. 1981. "Microwave Backscatter Dependence on Surface Roughness, Soil Moisture, and Soil Texture: Part III-Soil Tension." *IEEE Transactions on Geoscience and Remote Sensing* GE-19 (1): 51–61. doi:10.1109/TGRS.1981.350328.

Elhag, M. 2016. "Evaluation of Different Soil Salinity Mapping Using Remote Sensing Techniques in Arid Ecosystems, Saudi Arabia." *Journal of Sensors* 2016 (Jan): e7596175. doi:10.1155/2016/7596175.

Fallahi, S., M. H. Banaei, and Y. Eskandarzadeh. 1983. "Report of Semi-Detailed Studies of Soil Sience Qom-Masileh." *Soil and Water Research Institute, Iran. Technical Journal* 628: 1–149.

Fletcher, K. 2012. *Sentinel-1: ESA's Radar Observatory Mission for GMES Operational Services (ESA SP-1322/1 March 2012)*. Noordwijk: ESA Communications. ISBN:978-92-9221-418-0.

Gong, H., Y. Shao, B. Brisco, Q. Hu, and W. Tian. 2013. "Modeling the Dielectric Behavior of Saline Soil at Microwave Frequencies." *Canadian Journal of Remote Sensing* 39 (1): 17–26. doi:10.5589/m13-004.

Grissa, M., R. Abdelfattah, G. Mercier, M. Zribi, A. Chahbi, and Z. Lili-Chabaane. 2011. "Empirical Model for Soil Salinity Mapping from SAR Data." *2011 IEEE International Geoscience and Remote Sensing Symposium*, 1099–1102. doi:10.1109/IGARSS.2011.6049388.

Hasar, U. C., M. F. Akay, and S. N. Kharkovsky. 2003. "Determination of Complex Dielectric Permittivity of Loss Materials at Microwave Frequencies." *Mathematical and Computational Applications* 8 (3): 319–326. doi:10.3390/mca8030319.

Lasne, Y., P. Paillou, A. Freeman, T. Farr, K. C. McDonald, G. Ruffie, J. M. Malezieux, B. Chapman, and F. Demontoux. 2008. "Effect of Salinity on the Dielectric Properties of Geological Materials: Implication for Soil Moisture Detection by Means of Radar Remote Sensing." *IEEE Transactions on Geoscience and Remote Sensing* 46 (6): 1674–1688. doi:10.1109/TGRS.2008.916220.

Lee, J., K. W. Hoppel, S. A. Mango, and A. R. Miller. 1994. "Intensity and Phase Statistics of Multilook Polarimetric and Interferometric SAR Imagery." *IEEE Transactions on Geoscience and Remote Sensing* 32 (5): 1017–1028. doi:10.1109/36.312890.

Lee, J., and E. Pottier. 2009. "Polarimetric Radar Imaging: From Basics to Applications." In *Optical Science and Engineering 142,* edited by B. J. Thompson. Boca Raton: CRC Press.

Li, Y. Y., K. Zhao, Y. L. Ding, J. H. Ren, and Y. Li.2013."An Empirical Method for Soil Salinity and Moisture Inversion in West of Jilin." *Proceedings of the 2013 the International Conference on Remote Sensing, Environment and Transportation Engineering (RSETE 2013)*, 1921. Nanjing, China. 2628 vols. doi:10.2991/rsete.2013.5.

Li, Y. Y., K. Zhao, J. H. Ren, Y. L. Ding, and L. L. Wu. 2014. "Analysis of the Dielectric Constant of Saline-Alkali Soils and the Effect on Radar Backscattering Coefficient: A Case Study of Soda Alkaline Saline Soils in Western Jilin Province Using RADARSAT-2 Data." *The Scientific World Journal* 2014 (Jul.): e563015. doi:10.1155/2014/563015.

Materka, A., and M. Strzelecki. 1998. "Texture Analysis Methods–A Review." In *Technical University of Lodz, Institute of Electronics*, 9–11. Brussels: COST B11 report.

Metternicht, G., and J. A. Zinck., eds. 2009. *Remote Sensing of Soil Salinization: Impact on Land Management*. Boca Raton: CRC Press. doi:10.1201/9781420065039.pt1.

MirMazloumi, S. M., and M. R. Sahebi. 2016. "Assessment of Different Backscattering Models for Bare Soil Surface Parameters Estimation from SAR Data in Band C, L and P." *European Journal of Remote Sensing* 49 (1): 261–278. doi:10.5721/EuJRS20164915.

Remote Sensing Laboratory. 2018. "*Remote Sensing Lab*." *Remote Sensing Lab*. Accessed 15 July 2018. *http://rslab.ut.ac.ir/*.

Richards, L. A. 1954. "Diagnosis and Improvement of Saline and Alkali Soils." *Soil Science* 78 (2): 154. doi:10.1097/00010694-195408000-00012.

Saha, S. K. 2011. "Microwave Remote Sensing in Soil Quality Assessment." *ISPRS - International Archives of the Photogrammetry, Remote Sensing and Spatial Information Sciences* 3820 (Aug): 34–39. doi:10.5194/isprsarchives-XXXVIII-8-W20-34-2011.

Shao, Y., H. Guo, Q. Hu, Y. Lu, Q. Dong, and C. Han. 2003. "Effect of Dielectric Properties of Moist Salinized Soils on Backscattering Coefficients Extracted from RADARSAT Image." *IGARSS 2003. 2003 IEEE International Geoscience and Remote Sensing Symposium. Proceedings (IEEE Cat. No.03CH37477)*, edited by IEEE, 2789–2791. 4. doi:10.1109/IGARSS.2003.1294586.

Shrestha, D. P., and A. Farshad. 2009. "Mapping Salinity Hazard: An Integrated Application of Remote Sensing and Modeling-Based Techniques." *Remote Sensing of Soil Salinization. Impact on Land Management* 257. doi:10.1201/9781420065039.pt3.

Singh, G., D. S. Bundela, M. Sethi, K. Lal, and S. K. Kamra. 2010. "Remote Sensing and Geographic Information System for Appraisal of Salt-Affected Soils in India." *Journal of Environmental Quality* 39 (1): 5–15. doi:10.2134/jeq2009.0032.

Torres, R., P. Snoeij, D. Geudtner, D. Bibby, M. Davidson, E. Attema, P. Potin, et al. 2012. "GMES Sentinel-1 Mission." *Remote Sensing of Environment, the Sentinel Missions - New Opportunities for Science* 120 (May): 9–24. doi:10.1016/j.rse.2011.05.028.

Vapnik, V., S. E. Golowich, and A. Smola. 1996. "Support Vector Method for Function Approximation, Regression Estimation, and Signal Processing." In *Proceedings of the 9th International Conference on Neural Information Processing Systems (NIPS'96),* 281–287. Cambridge, MA: MIT Press. http://dl.acm.org/citation.cfm?id=2998981.2999021.

Vijayarekha, K. 2014. *Feature Extraction*. Thanjavur: School of Electrical and Electronics Engineering. SASTRA University.

Wu, W., A. S. Mhaimeed, W. M. Al-Shafie, F. Ziadat, B. Dhehibi, V. Nangia, and E. De Pauw. 2014. "Mapping Soil Salinity Changes Using Remote Sensing in Central Iraq." *Geoderma Regional* 2–3 (Nov): 21–31. doi:10.1016/j.geodrs.2014.09.002.

Wu, Y., and W. Wang. 2011. "Modelling the Backscattering Coefficient of Salt-Affected Soils Using AIEM Model." In *Earth Resources and Environmental Remote Sensing/GIS Applications II*, Vol. 8181, 81811O. International Society for Optics and Photonics. doi:10.1117/12.897933.